Chapter 7

Surface Energy and Wetting in Island Films

Sergei Dukarov, Aleksandr Kryshtal and
Vladimir Sukhov

Additional information is available at the end of the chapter

http://dx.doi.org/10.5772/60900

Abstract

The chapter describes the fundamental aspects of the effects of scale on surface phenomena in condensed films. Experimental and theoretical data for the size and temperature dependencies of the surface energy (including the solid phase); wetting of solid surfaces and free thin films by small metal particles are discussed. Several modern methods of contact angle measurement in small-sized systems based on the optical and electron microscopy methods are described.

Keywords: surface energy, small particles, thin films, wetting, size effects

1. Introduction

Surface energy is one of the most important characteristics of condensed matter. While methods available for the liquid phase enable to determine reliably not only the value but also the temperature dependence of surface energy [1–3], for the solid phase the accuracy of existing methods, as a rule, does not allow to trace its temperature dependence [4, 5]. Therefore, the following approach is justified: what information can be obtained about surface energy of the condensed matters on studies of various properties and processes in small size samples [6–9]. This article considers mainly the investigations of temperature and size dependence of surface energy of condensed matter based on the analysis of surface phenomena and phase transitions in nano-sized systems.

Wetting of solid surfaces with a liquid as well as spreading of a liquid over solid surfaces as a manifestation of interaction between the solid and liquid phases is one of the universal

phenomena and covers a wide variety of both fundamental and technological processes. Despite their crucial importance, these processes are still unclear [1, 2, 10]. Therefore, this paper focuses on effects of wetting in nanodispersed systems and considers various physical and chemical factors affecting it. Such statement of the problems seems actual since these details are important to describe a wide range of processes and phenomena, whereas the available data are disembodies and often ambiguous or even lacking.

2. The surface energy of nanoparticles

2.1. The size dependence of the surface energy of nanoparticles

In the framework of the Gibbs thermodynamics of heterophase systems, the size dependence of surface energy is due to the curvature of the phase interface. The Gibbs method applied to interfaces with a small curvature radius was first developed by Tolman [11], who derived the equation relating the surface energy σ of a spherical particle with its radius *R*

$$\frac{1}{\sigma}\frac{d\sigma}{dR} = \frac{\left(2\delta/R^2\right)\left(1+\delta/R+\delta^2/3R^2\right)}{1+\left(2\delta/R\right)\left(1+\delta/R+\delta^2/3R^2\right)} \tag{1}$$

where δ is the difference between the radii of equimolecular surface and surface of tension. Since the function $\delta = \delta(R)$ is unknown, at $\delta << R$ the variable δ can be considered constant and equal to the value for plane interface, that is, $\delta \approx \delta_\infty$. Under this assumption approximate solution to equation (1) was obtained in [11] known in literature as the Tolman formula:

$$\sigma/\sigma_\infty = 1/\left(1+2\delta_\infty/R\right)$$

For particles with $R >> \delta_\infty$ the first term of the expansion will be sufficient

$$\sigma = \sigma_\infty\left(1-\alpha/R\right). \tag{2}$$

In this approach the parameter $\alpha = 2\delta_\infty$ has a definite physical meaning as a width of the respective phase interface for any condensed phases. Character of the dependence $\sigma(R)$ is determined by the sign of the parameter δ_∞. In the case when $\delta_\infty > 0$, surface energy of microparticles will decrease, and at $\delta_\infty < 0$, conversely, increase of σ with decrease of *R*. Since the sign and value of parameter δ_∞ cannot be obtained based on thermodynamic prerequisites, determination of the type of the dependence $\sigma(R)$ calls for the use of the model of the structure of the transition layer for real systems or experimental results. In [3] this problem is solved for a simple idealized fluid using correlation function methods and it is shown that in this system the transition layer has a layered structure corresponding to some orderliness of particles therein. This is essential for many phenomena in surface physics.

Calculations of δ_∞ for plane liquid–vapor interfaces made by statistical methods [12] has shown that the quantity $\delta_\infty > 0$ and has a value of approximately a few tenth of nanometer (e.g., according to [12] for argon at 90 K $\delta_\infty = 0.36$ nm). Further research with use of a computer simulation [13–17], electron theory of surface energy of metals [18, 19], the thermodynamic perturbation theory [20, 21] is consistent with the results in terms of the type of the dependence $\sigma(R)$.

Qualitatively, the decrease in the surface energy of small particles can be explained as follows. For the condensed phase being in equilibrium with its own vapor, the interface surface energy at first approximation is proportional to the difference between the number of atoms (molecules) per unit volume of the condensed and vapor phases. With decreasing particle size of the condensed phase vapor pressure increases, and, consequently, its density increases, which causes decrease of the surface energy of the particle – saturated vapor interface approximately in inverse proportion to the particle radius.

In this way, theoretical studies suggest the existence of the size dependence of surface energy in the nanodispersed systems. According to estimates made using different methods, dependencies of σ on size for particles and films are manifested as a monotone decrease with decreasing size starting from a radius of less than 20 nm for particles and a thickness of < 5 nm for films.

2.2. Experimental foundations for the determination of surface energy of nanoparticles

Experimental determination of surface energy of solid bodies is a challenging task. Experimental methods available to scientists today offer the measurement of values of surface energy of liquid-phase matters with a reasonable degree of accuracy and in a broad temperature band, which is not the case for the crystalline phase. Known experimental methods for the determination of the surface energy for the crystalline phase are limited, and, as a rule, have a very narrow range of pre-melting temperatures and provide precision of not more than 10–20% [4]. This is largely due to the fact that surface energy is not a directly measurable value, but in most cases it is estimated as an adjustable parameter in various processes such as, for example, wetting, spreading, melting, crystallization, dissolution, analysis of high-temperature creep, electronic work function, etc. Among the best-known methods are the following: the crystal cleavage method, the dispersed powder dissolution method, the "neutral" droplet method, the multiphase equilibrium method, the growth and evaporation steps method, the "healing" scratch method, and, finally, the zero creep method [4]. Surface energy may also be evaluated by the measurement of electronic work function [18, 19]. However, the analysis of these methods shows that they are not applicable to the measurement of surface energies of small particles.

2.2.1. Kinetics of evaporation of small particles and surface energy

Surface energy of small particles can be determined by kinetics of evaporation in vacuum at a constant temperature [6]. The method is based on the concepts of the molecular-kinetic theory

that supposes that the rate of evaporation from a unit of free surface in vacuum is defined by the expression

$$\frac{dM}{dt} = \left(\frac{m}{2\pi kT}\right)^{1/2} P(T),$$

where m is mass of atom (molecule), k is Boltzmann constant, P is pressure of saturated vapor at temperature T. For the particle with the radius R saturated vapor pressure is linked to the vapor pressure over a flat surface $P_\infty(T)$ with the Kelvin equation

$$P(T,R) = P_\infty(T)\exp\left(\frac{2\mathrm{v_a}}{kT}\frac{\sigma}{R}\right). \tag{3}$$

($\mathrm{v_a}$ is atomic volume). The evaporation rate will be equal to

$$\frac{dM}{dt} = \left(\frac{m}{2\pi kT}\right)^{1/2} P_\infty(T)\exp\left(\frac{2\mathrm{v}_a}{kT}\frac{\sigma}{R}\right). \tag{4}$$

For an array of particles on the substrate it is more practicable to measure not the evaporation rate dM/dt, but the dependence of the particle radius on its evaporation time t at a constant temperature. From the relation of R to t one can determine the variation of the particle radius dR/dt at different R and, consequently, find σ. Indeed, as it follows from (4)

$$\left|\frac{dR}{dt}\right| = \frac{1}{\rho}\frac{dM}{dt} = \frac{1}{\rho}\left(\frac{m}{2\pi kT}\right)^{1/2} P_\infty\exp\left(\frac{2\mathrm{v}_a}{kT}\frac{\sigma}{R}\right) \text{ or } \ln\left|\frac{dR}{dt}\right| = \ln A + \frac{B\sigma}{R}, \tag{5}$$

where

$$A = \frac{1}{\rho}\left(\frac{m}{2\pi kT}\right)^{1/2} P_\infty(T) \text{ and } B = \frac{2\mathrm{v}_a}{kT}. \tag{6}$$

According to (5) and (6), knowing the temperature, particle size reduction rate dR/dt, and $P_\infty(T)$, one can determine the value of σ. These expressions adequately describe evaporation kinetics of liquid Pb particles and crystalline Ag particles [6] at values of σ close to handbook ones.

Electron microscope investigation of the kinetics of particle evaporation was later used to register the melting temperature of small crystalline Au particles by breaks in dependencies $R(t)$ [7]. This effect is due to the difference in evaporation rates for crystalline and liquid states.

http://dx.doi.org/10.5772/60900

The melting temperature lowering data obtained for small Au particles from their evaporation kinetics [7] correlate well with similar results established later using electron diffraction analysis [22]. Investigating the kinetics of evaporation of silver particles on carbon substrates has shown that the observed sublimation temperature generally decreased with decreasing particle size [23], in agreement with the predictions from the Kelvin equation. However, sublimation of smaller nanoparticles was often observed to occur in discrete steps, which led to faceting of the nanoparticles.

This method was used to determine the surface energy of small particles in Bi, Pb, and Au island films [8, 9]. The sample film was heated in the electron microscope by electron beam up to the onset temperatures of evaporation. The temperature and, hence, evaporation rate was controlled with beam density. The particles radius variation rate $\Delta R/\Delta t$ during evaporation was established by the analysis of a series of successive electron micrographs taken at fixed time intervals. These data allowed to establish the temperature of particles heated by the electron beam. For this purpose, expression (6) at $R \to \infty$ should be represented in the form

$$\lg P_{\infty}(T) = \lg C + 1/2 \ \lg T, \tag{7}$$

Where $C = \rho\left(\frac{2\pi k}{m}\right)^{1/2} (dR/dt)_{R\to\infty}$.

Tabular data are available for the function $P_{\infty}(T)$, while the value $(dR/dt)_{R\to\infty}$ is to be determined experimentally from the results of change of the radius of the particles during their evaporation represented in accordance with (5) and (6) in the coordinates "ln $|\Delta R/\Delta t|$ — $1/R$." Equation (7) can be solved graphically for T and, thus, the temperature of the observed object can be found.

Figure 1a presents an example of a series of successive micrographs of Bi island films obtained in the process of their evaporation with the time interval of 15 s, and Figure 1b, c present the results of analysis of evaporation of Au island films. These data were used to find values of ΔR for different-sized particles at fixed time intervals Δt. Resulting dependencies for the ensemble of particles in Au island films (the size range of 10–50 nm) are presented in Figure 1c in the coordinates "ln $|\Delta R/\Delta t|$ — $1/R$." Since these dependencies are linear, according to (5) and (6) they allow us to establish σ and values of $(dR/dt)_{R\to\infty}$. The range of particle sizes in experiments [8, 9] made 10–150 nm. For Pb and Bi temperatures of particle evaporation were higher than melting temperatures, whereas for Au island films data on evaporation rates both in liquid and crystalline state were obtained.

Values of surface energies σ for Au, Pb, and Bi found as a result of the preceding experiments are presented in Table 1, which also presents available literature data for σ at similar temperatures. Comparison of values of σ obtained by kinetics of evaporation of small particles with available data for bulk samples shows their satisfactory fit.

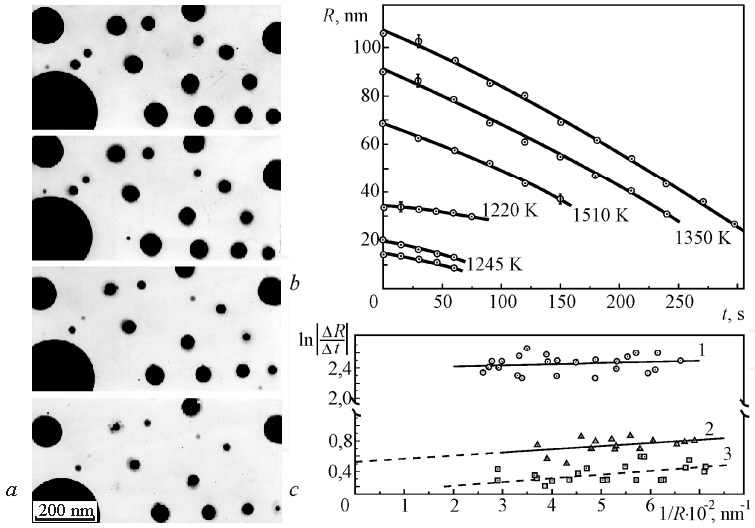

Figure 1. Electron micrographs of successive stages of evaporation of Bi island films on amorphous Si films (a); change of particle size in the process of evaporation (temperatures are given in the charts) (b), and relations of evaporation rate to reciprocal size of particles for gold island films on carbon substrates (c)

Me	Evaporation kinetics [8, 9]		Literature data	
	T, K	σ, mJ/m²	*T*, K	σ, mJ/m²
Au	1245	1410±20	1240	1410 [5]
	1260	1430	1176–1306	1390±80 [5]
	1310	1320±100	1297	1137 [6]
	1350	1230±100	1348	1135 [6]
	1510	1160		
Pb	670	385	557–589	560 [5]
	720	484	735	438 [7]
	740	452	730	439 [7]
	750	450	748	436 [7]
	770	447		
Bi	650	386	509–518	501 [5]

Table 1. Comparison of surface energy values for Au, Pb, and Bi [8]

http://dx.doi.org/10.5772/60900

2.2.2. Dependence of surface energy on particle size

Available experimental data, for example, [8, 9, 24, 25], offer contradictory conclusions regarding the sign of the size dependence of the surface energy of small particles.

The preceding paragraph demonstrates that the surface energy of small particles can be directly determined using the kinetics of their evaporation in vacuum. Table 1 presents the results of such experiments for nanoparticles over 20 nm in size. At the same time, the kinetics of evaporation of Pb and Au nanoparticles with the size below 20 nm both in liquid and crystalline state was investigated in works [6, 7]. The authors of these studies used these results to test the applicability of the Kelvin equation (3) and to estimate values of σ at temperatures at which the evaporation of particles is observed. However, the authors [6, 7] did not analyze the dependence of particle evaporation rates on particle size. Such analysis was offered by the authors in [8, 9], where they demonstrate that for particles with a size of less than 10 nm their surface energy decreases. Figure 2a presents an example of the plot of $R(t)$ for Pb particles at different temperatures, and Figure 2b presents particle size reduction rate in the coordinates "$\ln | \Delta R / \Delta t | - 1 / R$" plotted using these data.

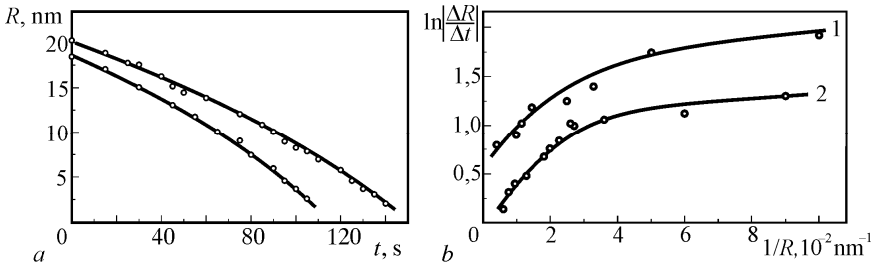

Figure 2. Change of the radius of Pb particles in the process of evaporation (a) and the plot of their evaporation rate against size on the coordinate "ln | ΔR/Δt | — 1/R" (b) (calculated using data [7]). Curves 1, 2 correspond to particles of different initial size at T = 720 K

It is evident that at sizes of particles less than 10 nm significant deviation of the preceding relationship from linear is observed, which in accordance to (5) is an evidence of decreasing σ. Values of σ calculated using expression (5) are presented in Figure 3 (Curve 5), which also shows calculation data of the relation $\sigma(R)$ for Pb microparticles using the Tolman equation (2) with the parameter α = 0.29 nm, which value is determined from the empirical relation $\alpha = 0.916 v_a^{1/3}$ [26] (Curve 4). The same figure presents the results of calculation of values of gold and lead nanoparticles surface energy at different temperatures (Curves 2, 3, 5) obtained from the data of analysis of particle evaporation kinetics given in [6, 7].

Comparison of these dependencies produces qualitatively the same result, that is, the surface energy of small particles decreases with decrease of their size, but nanoparticles evaporation experiments suggest a stronger relationship $\sigma(R)$.

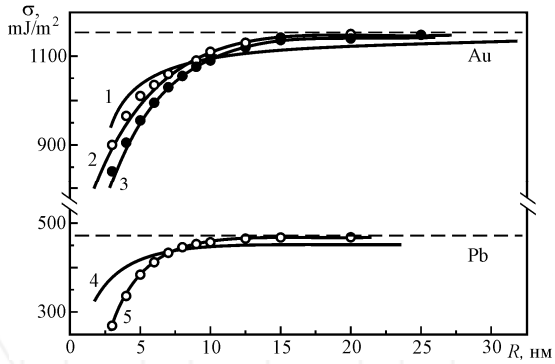

Figure 3. The plot of surface energy against microparticles size: a – Au (1 – calculation using the Tolman equation at α = 0.24 nm, 2 and 3 – using microparticles evaporation data at T = 1348 K and T = 1316 K); b – Pb (4 – calculation using the Tolman equation at α =0.29 nm, 5 – particle evaporation data at T = 735 K)

2.2.3. Decrease in small particles melting temperature and surface energy

It is common knowledge that melting temperature of small particles, thin metal, and alloy films is a function of size [6, 7, 22, 27–36]. When considered in terms of thermodynamics, there exist several models to describe the size dependence of melting temperature of small particles [27]; however, as the quantitative analysis of experimental data shows, the triple point model proves to be the most feasible. Within the framework of this model the problem of the melting temperature of the small particle was first solved by Pavlov [37], who obtained expression for the size dependence of melting temperature

$$\frac{T_S - T_R}{T_S} = \frac{3}{\lambda R}\left(\sigma_S - \sigma_l\left(\rho_l \Big/ \rho_s\right)^{1/3}\right), \tag{8}$$

where T_S and T_R are the melting temperatures of a bulk sample and a particle with the radius R, λ is melting heat, σ and ρ are surface energies and densities of crystalline (s) and liquid (l) phases, respectively. As it is seen from (8) using experimental data $T_R(R)$, one can establish the difference of surface energies of solid and liquid phases, that is, $\Delta\Omega=\sigma_S-\sigma_l\,(\rho_l/\rho_S)^{1/3}$, and given known values of σ_l find σ_S. The possibility of determining surface energy in solid phase and its temperature dependence using experimental data $T_R(R)$ are detailed in work [9]. It is possible since the difference $\Delta\Omega$ is not a constant value, but changes in accordance to variation of σ_S and σ_l. Considering this, the expression for the melting temperature of small particles can be represented in the following form

$$\frac{T_s - T_r}{T_s} = \frac{3\Delta\Omega_0}{\lambda\left(R - \Delta R\right)}, \tag{9}$$

http://dx.doi.org/10.5772/60900

where $\Delta\Omega_0 = \sigma_s^0 - \sigma_l^0(1 + \delta_V / 3)$ is the variation of surface energy during melting at temperature T_s; $\Delta R = 3T_s[\gamma_l(1 + \delta_V/3) - \gamma_s]/\lambda\rho_s$, $\gamma_l = \partial\sigma_l/\partial T$ is the temperature coefficient of liquid phase surface energy; $\gamma_s = \partial\sigma_s/\partial T$ is the temperature coefficient of solid phase surface energy, σ^0 is surface energy of relevant phase at bulk sample melting temperature T_s, δ_V is relative variation of volume during melting.

It follows from (9) that using the experimental relation $T_R(R)$ one can calculate $\Delta\Omega$ at different temperatures and, provided known type of temperature dependence of liquid phase surface energy $\sigma_l(T)$ below T_s, find dependence $\sigma_s(T)$. This approach allowed to evaluate relations $\Delta\Omega(T)$ and $\sigma_s(T)$ over a broad temperature interval using experimental data of $T_R(R)$ for Sn and In [31, 32]. The validity of linear extrapolation of values of liquid phase surface energy σ_l to the region of significant supercooling was substantiated in works [9, 38].

Considering the preceding, we calculated values of surface energies for a number of metals (In, Sn, Bi, Pb, Al, Au) in crystalline state over the temperature interval of (0.6–1)T_s. The obtained results are presented in Figure 4. These values agree well with available literature data on σ_s for bulk samples obtained by other methods.

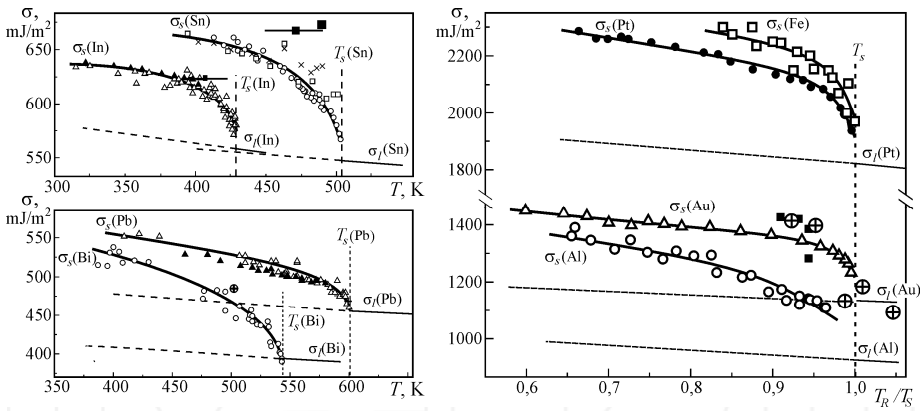

Figure 4. Surface energy temperature dependence for different metals according to the $T_R(R)$ data [6, 7, 22, 31–36] (the dotted lines are extrapolation of dependencies $\sigma_l(T)$ to the area of supercooling state) ■ – creep data [5], ⊕ – small particles evaporation data [7], □ – data for Fe [39]

It is evident that there is a common tendency observed for all of the preceding metals manifested in the fact that the values of σ_s have nonlinear temperature dependence. With relative temperatures below $T/T_s \leq (0.85–0.9)$ the temperature coefficient for these metals becomes approximately constant and makes module (0.3–0.4) mJ/m²K (Figure 4). Nonlinear decrease in σ_s at $T \to T_s$ is probably common for metals. The result of work [39] supports this assumption. In this work, surface energy of macroscopic iron samples is determined using the method of wetted solid surface deformation over the range of temperatures (1580–1790) K (Figure 4).

The nonlinear increment effect $|\partial\sigma_S/\partial T|$ at $T \to T_S$ was considered for In and Sn and supported by case study calculations of σ_S, made for Bi, Pb, Al, Au in work [9]. A detailed analysis of nonlinear relation of the temperature coefficient $\partial\sigma_S/\partial T$ in premelting temperature band showed its vacancy nature [9]. Based on the analysis of data on $\sigma_S(T)$ in the coordinates "$\ln(\Delta\sigma/\sigma) - 1/T$" the paper also estimated the vacancy formation energy E_V that yielded the following values: In – 0.5 eV, Sn – 0.62 eV and Pb – 0.6 eV. Close values of the values of E_V support vacancy mechanism of nonlinear temperature dependence of solid phase surface energy in the premelting temperature band.

3. Wetting in condensed films

Information on values of surface energy and interfacial energy of contacting phases can be obtained when studying wetting in solid–liquid systems. Analysis of known methods for the determination of the wetting contact angles θ shows that the use of traditional methods [1, 40] for studying wetting in ultradispersed systems is quite limited. In view of these, new methods [41, 42] were developed that allowed to investigate wetting in ultradispersed systems with different types of contact interaction (i.e., applicable both at $\theta < 90°$, and for $\theta > 90°$), with typical phase size changing over a broad range.

Test samples were island films of various metals condensed in vacuum by vapor–liquid method on solid substrates, which, as a rule, were prepared using vacuum condensation as well [9, 42–44]. The substance substrate was deposited on the NaCl (or KCl) cleavages in a vacuum of 10^{-7}–10^{-9} mm Hg. After that the investigated metal was condensed at a substrate temperature that ensured condensation of the metal into liquid phase. The obtained films were cooled in vacuum to room temperature and the crystallized particles were further analyzed using the methods of optical, scanning, and transmission electron microscopy. According to the estimates and data of experimental research [42–44] (Figure 5) contact angle measurement error due to changing droplet volume during its solidification on the substrate is not more than 2°. In this way one can discard the variation of the angle during crystallization of liquid droplets and relate the values of θ found for crystallized particles to values of the contact angles of liquid droplets at the temperature of their formation.

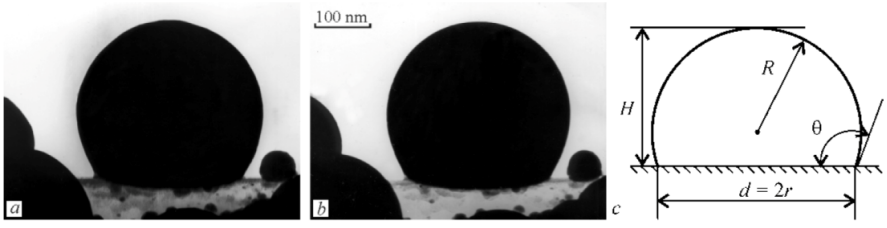

Figure 5. Electron microscope images of crystalline (a) and liquid (b) lead particles on a carbon substrate and a schematic representation of a liquid droplet on a solid substrate (c)

http://dx.doi.org/10.5772/60900

In the case when the gravity effect can be disregarded, the shape of small droplets is a segment of a sphere (estimations show that this is knowingly true for metals with particle size below 10^5 nm). To find the angle θ it is sufficient to measure any two of the three quantities that define droplets on the substrate: the radius of droplet surface curvature R, the diameter of its base d ($d = 2r$), and the height H (Figure 5c).

The methods suggested in [41, 42] differ in approaches to measure geometric parameters of droplets. The most frequently used cleavage and convolution methods are based on measurement of the said parameters during direct observation of droplet profiles with an optical or electron microscope [41, 42]. In this case, the contact angle is determined from the relations

$$\theta = 2\,\mathrm{arctg}\frac{2H}{d} = \arccos\left(1-\frac{H}{R}\right) = \begin{cases} \arcsin\dfrac{d}{2R}, & \theta < 90°, \\ 180° - \arcsin\dfrac{d}{2R}, & \theta > 90°. \end{cases}$$

The developed complex of methods [41, 42] makes it possible to investigate the wetting of surfaces with small droplets, with the size of the latter ranging within 3–10^5 nm.

3.1. Size effect in wetting

Wetting in the liquid–solid system is defined by the equilibrium contact angle θ, which is related to surface energies of contact phases with Young's equation

$$\cos\theta = \left(\sigma_u - \sigma_{ul}\right)/\sigma_l, \tag{10}$$

where the indices u and l refer to solid (substrate) and liquid (particle) phase, respectively. One would expect that the size dependence of surface energy will cause a difference of wetting patterns in nanodispersed systems from known ones for macroscopic objects. This may change the contact angle with increasing dispersity of both liquid and solid phases. In order to provide a theoretical description of these phenomena, it is necessary to solve the problem of the equilibrium shape of the microdroplet and its contact angle, that is, obtain an equation analogous to Young's equation (10) with regard for the relationship $\sigma(R)$.

Consider, following [42, 43, 45], a small droplet of liquid on a flat solid surface. The total free energy of the system F is comprised of the hydrostatic energy pV (here, pressure p may be regarded as the undetermined Lagrange multiplier that accounts the constant droplet volume V) and surface forces energy

$$F = -pV + \int_{S_l} \sigma_l dS + \int_{S_{ul}} \left(\sigma_{ul} - \sigma_u\right) dS, \tag{11}$$

where S is the interfacial area.

In accordance with existing concepts [11, 45] the surface energy σ_l is viewed as dependent on the average surface curvature C at a given point

$$\sigma_l = \sigma_l^{\infty}\left(1 - \alpha C\right). \tag{12}$$

For spherical surface ($C = 1/R$) relation (12) agrees with expression (2) known in the literature as the Tolman formula.

When finding equilibrium conditions, one should take account of the size dependence of the interfacial energy of droplet – substrate boundary σ_{ul}. It would be natural to consider this dependence as a relation not to the radius of the surface curvature R, but to the radius of the wetted perimeter r [42, 45], that is, for σ_{ul} use relationship in the form

$$\sigma_{ul} = \sigma_{ul}^{\infty}\left(1 - \beta/r\right). \tag{13}$$

Expressions (12) and (13) apply at $1/C >> \alpha$ and $r >> \beta$. Finding equilibrium characteristics of the droplet does not require any assumptions as to the sign and value of parameters α and β.

Due to the axiality of the problem, it can be solved using polar coordinates with their origin in the center of the circle of the wetted perimeter and the vertical axis z perpendicular to the substrate plane. The profile of the free surface of the droplet is defined by the function $z(\rho)$. Without loss of generality, one can regard $z(\rho)$ function as single-valued, that is, consider the case of $\theta < 90°$ (it can be shown that the obtained results will be valid on the whole range of angles θ, if z is chosen as an independent variable and the droplet surface is set single-valued at any θ using the function $\rho(z)$).

The equilibrium shape of the droplet is found by minimizing the functional (11), which, with regard to relations for droplet volume and areas of its boundary surfaces, is written as follows:

$$\begin{aligned} F &= 2\pi\int_0^r \left[-pz + \sigma_l(C)\left(1+z'^2\right)^{1/2} + \sigma_{ul}(r) - \sigma_u\right]\rho d\rho, \\ C &= -\frac{1}{2}\left\{z''\left(1+z'^2\right)^{-3/2} + \frac{z'}{\rho}\left(1+z'^2\right)^{-1/2}\right\}. \end{aligned} \tag{14}$$

The summand $(\sigma_{ul}(r) - \sigma_u)\rho$ in the expression under the integral sign does not contain $z(\rho)$ and its derivatives, that is, the relation $\sigma_{ul}(r)$ defines only boundary conditions and has no effect on the shape of the droplet.

Functional variation (14) in δz gives the Euler equation, which after term-by-term integration takes on the form

$$-\frac{p\rho^2}{2}=\rho\left(1+z'^2\right)^{1/2}\frac{d\sigma_l}{dC}\frac{\partial C}{\partial z'}+\frac{\sigma_l\rho z'}{\left(1+z'^2\right)^{1/2}}-\frac{d}{d\rho}\left[\rho\left(1+z'^2\right)^{1/2}\frac{d\sigma_l}{dC}\frac{\partial C}{\partial z''}\right]. \tag{15}$$

The integration constant in (15) is equal to zero from the equal-zero condition of one of the non-integral summands δF at the point $\rho = 0$. The complexity of equation (15) makes its general solution unlikely, which fact urges us to use specification of relation σl(C) in the form (12). Substitution in (15) of relation (12) and expressions for derivatives $d\sigma_l/dC$, $\partial C/\partial z'$ and $\partial C/\partial z''$ yields a nonlinear differential first-order equation

$$\left[z'\left(1+z'^2\right)^{-1/2}\right]^2+\frac{2\rho}{\alpha}\left[z'\left(1+z'^2\right)^{-1/2}\right]+\frac{p\rho^2}{\alpha\sigma_l}=0,$$

which solution by separation of variables gives equilibrium shape of the droplet surface in the form of a sphere truncated by plane $z = 0$:

$$\left(z-z_0\right)^2+\rho^2=R^2. \tag{16}$$

The sphere radius satisfies the relation

$$p=\frac{2\sigma_l^{\infty}}{R}\left(1-\frac{\alpha}{2R}\right),$$

which shows that the undetermined Lagrange multiplier p is nothing, but the Laplace pressure adjusted for the dependence σ(*R*). Integration constant $z_0=\pm\sqrt{R^2-r^2}$ has the meaning of z-coordinate of the sphere center (16) and is determined from the condition $z(r) = 0$.

The wetting angle θ can be found from the boundary condition or, since function $z(\rho)$ is defined, from the condition of minimum free energy of the droplet at a constant volume. For this purpose the surface energy of the droplet must be expressed in terms of *R* and θ

$$F_s=\pi R^2\left\{2\sigma_l\left(R\right)\left(1-\cos\theta\right)+\left[\sigma_{ul}(r)-\sigma_u\right]\sin^2\theta\right\}.$$

By setting the derivative dF_s/dR to zero we can obtain the equation, which, considering constant volume, gives the equilibrium condition of a microdroplet on a substrate

$$\cos\theta=\left(\sigma_u-\sigma_{ul}-R\frac{d\sigma_l}{dR}-\frac{r}{2}\frac{d\sigma_{ul}}{dr}\right)\Big/\left(\sigma_l+R\frac{d\sigma_l}{dR}\right). \tag{17}$$

Equation (17), naturally, is different from Young's equation (10) by presence of summands containing surface energy derivatives with respect to size.

By using expressions (12) and (13) for $\sigma_l(R)$ and $\sigma_{ul}(R)$, we can write the relation for the contact angle of the microparticle through the parameters α and β that define the size dependence of respective surface energies as follows [42, 45]:

$$\cos\theta = \cos\theta_\infty - \frac{\alpha}{R} + \frac{\beta}{2R}\frac{\sigma_{ul}^\infty}{\sigma_l^\infty}\frac{1}{\sin\theta}. \tag{18}$$

Naturally, in the extreme case at $\sigma \to \sigma^\infty$ ($\alpha/R \to 0$, $\beta/R \to 0$) all the expressions received go into known relations of the capillary theory. It should be further noted that equation (18) agrees by the type of functional dependence on size with relations received in the scope of the line tension model [46, 47].

3.1.1. Contact angle size dependencies and surface energy of the solid–liquid interface

The size effect in wetting of the flat surface of the solid substrate with small metal droplets was first found for vacuum-condensed island tin and indium on an amorphous carbon substrate [42–44]. A combination of optical and electron microscopy [41, 42] allowed to determine wetting contact angles over the range of particles of 1–10^4 nm. According to measurements using optical microscopy the contact angle in the Sn/C system for micron-sized droplets is constant and makes 151°±2°, which fact agrees with the known data for the tin-carbon system. For measurement of contact angle in islands of smaller size we applied the methods of convolution and photometric analysis of electron microscope pictures.

The results of measurement of θ for tin on carbon substrate are presented in Figure 6a, which demonstrates that for big particles (R > 30 nm) values obtained are close to respective values of micron-sized droplets. As the size of the particles decreases (R < 30 nm) one can observe decrease of the contact angle.

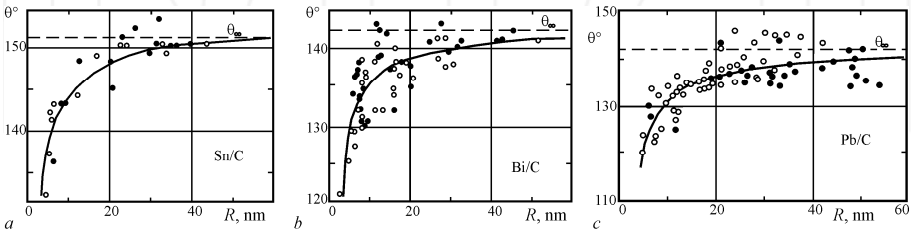

Figure 6. The plots of the contact angle against the radius of particles of tin (a), bismuth (b), and led (c) on a carbon substrate (O – data using convolution method, ● – using photometric measurement of electron microscope pictures) [9, 42–44]

The preceding research was followed later by the study of wetting in the systems of "island metal (Bi, Pb, Au) film–amorphous carbon film" and "Pb–amorphous silicon film" depending on the size of particles [9, 42–44]. For all investigated systems it was obtained that with particle sizes $R > 100$ nm and thicknesses of carbon and silicon films $t > 20$ nm, contact angles of liquid droplets in island films well agree with data of respective contact systems in bulk state. With particle sizes $R < 30$ nm the value θ decreases so that $\Delta\theta = \theta_\infty - \theta \approx (20°–25°)$ at $R = (4–5)$ nm (Figure 6). The conclusion regarding reduction of the contact angles of nanosized droplets to the extent of their spreading was obtained in [48] by modeling using the molecular dynamics method.

Influence of sample preparation conditions on the contact angles of microparticles in the gold–carbon system was discussed in detail in [50]. It showed that the amount of pressure of residual gases during the preparation of gold island films has no effect on the values of surface energies corresponding to the bulk state, though it has a slight impact on their size dependence.

The results of the study of wetting obtained [9, 42–44] and presented in Figure 6 are of separate interest, in particular, for some practical applications (e.g., the formation of ordered nanostructures by film melting [51–53]), but at the same time allow to obtain new physical information regarding properties of microparticles. Thus, using the experimental relations $\theta(R)$ and $\sigma_l(R)$ one can establish the size dependence of interfacial energy of the microparticle–substrate boundary σ_{ul}.

For analysis of results of the size effect of wetting in island films expression (18) was used, from which, using the relation $\theta(R)$ at known quantities of the parameter α and the value of the surface energy σ_u, the value of the interfacial energy of the microparticle–substrate boundary and its size dependence were found. The parameter α can be found from data on the kinetics of evaporation of small particles [8]. It may be evaluated using the relation $\alpha \approx 0.916 v_a^{1/3}$ (v_a – atomic volume) too [26]. Calculation of α using this relation yields the value of $\alpha(Pb) = 0.27$ and $\alpha(Au) = 0.23$ nm, that is, quantities close to those found experimentally in [8]. This allows to use at first approximation the preceding relation to estimate the parameter α for metals that lack experimental data for the relation $\sigma_l(R)$. The value of the surface energy of carbon film was determined and presented in work [9, 43] from the data on wetting of free films of different thickness with microdroplets of indium, tin, and lead, which makes $\sigma_u = 120 \pm 30$ mJ/m^2.

Using these data authors of work [45] found values of σ_{ul} and the parameter β, which are presented for the investigated metal-carbon systems in Table 2.

The parameters α and β are positive, which is an evidence of decreasing surface energy of microparticles and interfacial energy at the substrate boundary with a decrease of the radius. Values of α approximately correspond to the thickness of the surface layer at the liquid–vacuum boundary. The value β, which defines the width of the transition zone between the liquid particle and the substrate and depends on the nature of contacting phases, is 2–4 times as big as α.

Metal	σ_l^{∞}, mJ/m²	α, nm		σ_{ul}^{∞}, mJ/m²	β, nm	θ_{∞}
		Calculated	Experiment [8]			
Au	1130	0.24	0.23	955	1.0	138.4
Sn	531	0.28	-	574	0.53	152.4
Pb	450	0.29	0.27	463	0.91	140.9
Bi	376	0.30	-	407	0.5	141.0
In	559	0.27	-	566	0.55	143

Table 2. Results of wetting size effect in metal-carbon systems [42, 43, 45]

3.1.2. Wetting hysteresis in condensed microdroplets

The observed reduction of the contact angle θ with decreasing radius of the droplet is accounted for by the size dependence σ_l and σ_{lu}, due to the growing relative contribution of interface regions. However, wetting parameters are also subject to the influence of substrate elastic deformation, which was disregarded earlier when deriving equations (17) and (18). The effect of deformation on angle θ in the case when substrate is a thin film was dealt in detail in [54], for elastic half-space in [55], but because of approximation, the results presented in [55] cannot be applied to droplets with the size below 20–50 nm, that is, when wetting size effect is observed. Works [42, 56] offer solutions of the problem of determination of the value of the equilibrium wetting angle θ for the microdroplet with a radius of less than 50 nm with regard to elastic deformation of the substrate. On assumption that the force of liquid tension along the wetting perimeter is uniformly distributed along the ring of finite width, it was shown that elastic deformation effect is insufficient (1–2° for the systems considered earlier), and, hence, reduction of the contact angle is primarily defined by the size dependence of specific energies of interface surfaces. Nevertheless, for substrates with low value of Young's modulus ($E \sim 10^9$ N/m²) additional deflection of contact angle for small droplets reaches 5–6°.

At the same time, as a result of the small size of droplets and increased diffusion coefficients in nanodispersed systems [57–59], the wetting perimeter under the action of surface tension forces may experience irreversible changes, which may be registered with electron microscopy as circular traces on the substrate left after evaporated droplets. In addition, the plot of the radius of evaporating droplet against time at constant temperature, as a rule, has periodic deviations of experimental points from the continuous curve. Works dedicated to direct measurement of the wetting contact angle also demonstrate fluctuations $\Delta\theta \approx 10–15°$, while the precision of the convolution and photometry methods makes 3–5° [41, 42]. In both cases these deviations may be accounted for by wetting hysteresis. This phenomenon consists in fixation of the wetting perimeter, which under certain conditions, for example, during evaporation, significantly changes the behavior of the liquid droplet. Work [60] examines the reasons causing this effect in microdroplets, it analyses the effect of wetting hysteresis on parameters of the droplet–substrate system.

A number of works were concerned with wetting hysteresis, for example [46, 61], and the commonest causes of this effect are considered to be microroughness and inhomogeneity of the substrate. However, many assumptions underlying these works, for example, the roughness height of ~ 1 μm cannot be applied to microdroplets. In several systems fixation of the wetting perimeter is achieved by partial mutual dissolution of solid and liquid phases. Nevertheless, hysteresis may be as well observed for systems with minor mutual solubility, such as Au/C. Some authors noted that at high temperatures under the action of liquid surface tension forces, the substrate may be subject to inelastic deformation. In this case the triple contact area develops a prominent welt. Comparison of different mechanisms of mass transfer at small (~10^{-8} m) distances implies a conclusion about the defining role of surface diffusion. As follows from estimations made in work [60] characteristic time of deformation in the Au/C systems makes about 0.1 s. Since the time of condensation of films is about 10^2 s, in the process of droplet growth the welt has enough time to form even with quite frequent jumps of the wetting perimeter, that is, the droplet creates substrate roughness itself.

The values of the contact angles corresponding to perimeter breakdown with changing volume of the droplet were received [60] from the condition of the system's minimum free energy taking into account elastic deformations of the substrate and their partial relaxation in the triple contact area trough surface diffusion. According to [60] the contribution of relaxed elastic deformation energy reaches significant values, for example, for the Au/C system the wetting hysteresis, that is, difference between advancing θ_a and receding θ_r contact angles makes about 3°.

In this way, with changes of the volume of the droplet, for example, during evaporation, its wetting perimeter will be fixed until the contact angle is reduced to the critical value θ_r. Upon this wetting the perimeter will break, and the droplet will take the position corresponding to equilibrium (Young's) value θ_0. In this position the wetted perimeter develops a new welt and the process recurs. It may be noted that for sufficiently big droplets (with their base radius considerably larger than the width of the welt) the dependence of values of the angles θ_r and θ_a on the size is small. Thus, for the Au/C system with the droplet radius growing from 20 to 1000 nm the value of these angles changes by 1° due to the increase of elastic energy contribution.

Considerable amount of Laplace pressure in very small (less than 10 nm) droplets results in elastic deformation being able to relax not only in the triple contact area, but also directly under the droplet. In this case, along with the welt along the wetted perimeter dimples may form under the droplet, which causes higher hysteresis value, with the difference $\theta_0 - \theta_r$ growing much faster than $\theta_a - \theta_0$, that is, the minimum contact angles diverge from the equilibrium value more than the maximum ones. Taking into account the decrease of the value of the contact angle, one may conclude that, for example, for the same Au/C system the contact angle of small (2–5 nm) droplets may reach 65–70° at $\theta_0 = 138°$.

3.2. Wetting in droplet–thin film–substrate systems

Among the factors that define wetting in dispersed metal–metal systems, in addition to size effect of wetting, one can single out the following: discontinuity of intermediate film and

resulting heterogeneity of the substrate, mutual solubility of components in each other, formation of chemical compounds at the solid and liquid phase interface, and oxidation of the metal film. Therefore, wetting processes in ultradispersed systems are defined by a number of parameters, which are quite inseparable.

A case study research of the influence of fineness of the solid phase on the contact angle is presented in work [62], which investigated wetting of thin films of different thickness deposited on bulk substrate. It showed that in the melt (Ag, Cu, Sn, Pb)–metal film (Mo, V, Fe)–nonmetal substrate (sapphire, quartz, graphite) system the contact angle is subject to linear variation within the range of values corresponding to wetting of clean substrate (at thickness of film $t \rightarrow 0$) and wetting of film substance in compact state (at $t > t_c$). The values of critical thicknesses t_c, below which change of the contact angle is observed for the investigated systems is in the range of 20–50 nm. At the same, when carbon film covered germanium is wetted with tin the change of the contact angle is observed up to a thickness of 3 nm, while remaining unchanged further, and corresponds to the wetting of compact graphite. The authors explain the obtained results by discontinuity of carbon films at t < 3 nm.

Wetting in triple systems Pb/Ni/[NaCl, Si, GaAs], Sn/[C, Al, Al_2O_3]/KCl, Bi/Fe/KCl as a function of metal film thickness (2 nm < t < 200 nm) was investigated in [9, 42–44, 63]. These systems substantially differ by interaction behaviors: Sn–C, Sn–Al_2O_3, Bi–Fe – complete insolubility in solid and liquid states; Sn–Al – solubility 0.5 wt. % Al in Sn; and Pb–Ni – up to 4 wt. % Ni in Pb. Test samples were prepared as follows. Variable thickness intermediate film (Al, Fe, Ni, C, Al_2O_3) was condensed on monocrystal substrates (KCl, NaCl, Si, GaAs) in a vacuum of 10^{-6}–10^{-8} mm Hg. The studied metal (Sn, Bi, Pb) was condensed on this film by the vapor–liquid mechanism without deterioration in vacuum. The substrate temperature during condensation was 653 K for Pb, 523 K for Sn, and 560 K for Bi.

In all investigated systems degree of wetting strongly depends on intermediate film thickness, though the range of thicknesses, on which change of θ occurs is different. The common feature for the analyzed systems is that the contact angle is defined at a fist approximation by heterogeneity of the wetted surface and changes within extreme limits corresponding to wetting of clean substrate ($t \rightarrow 0$) and intermediate film material in bulk state ($t > t_c$). The critical thickness t_c, at which complete screening of a bulk substrate by a thin film is observed, depends on the character of interaction of the systems' components and varies from nanometers (no interaction) to tens and hundreds of nanometers (dissolution of the film in the melt, formation of chemical compounds). The analysis of the obtained results together with data [62] allowed to classify the main types of the relations $\theta(t)$ for wetting with a melt of thin film on the surface of a bulk substrate (Figure 7):

a. **Noninteracting systems** – Figure 7a. The value t_k in such systems is defined by the microstructure of intermediate film and to some extent may depend on technological parameters of its production (substrate temperature, condensation rate, etc.). The variation of the contact angle is defined by transition from discontinuous to continuous film and the dependence of its surface energy on thickness. Sn/C/KCl (Figure 8a), Sn/Al_2O_3/KCl, Sn/C/Ge [62] may serve as examples of such systems. Since wetting angle in such systems changes for intermediate film thinner than 10 nm, effects related to size variation

http://dx.doi.org/10.5772/60900

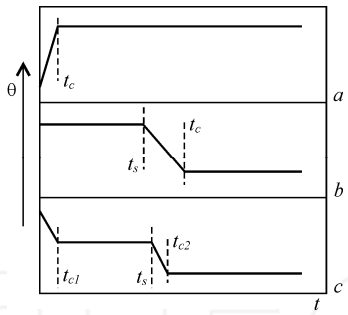

Figure 7. Main types of dependencies θ(t) for systems melt – film – substrate: a) noninteracting systems; b) systems with dissolution of film in the melt; c) systems with chemical interaction at the film–substrate interface

of film surface energy are also possible. Thus, in the Sn/C/KCl system variation of θ is observed in the range of $2 < t < 7$ nm. At the same time, electron microscope analysis of clean carbon films suggests their continuity with decrease of thickness down to 1.5–2 nm. This gives ground to assumption that apart from discontinuity of carbon film the relation $\theta(t)$ in the Sn/C/KCl system is also stipulated by their surface energy. Since with decreasing t changes not only σ_u, but also interface energies of the film–particle interface σ_{lu} and film–bulk substrate, the said relation, strictly speaking, reflects changes in adhesion tension σ_u–σ_{lu} with decrease of thickness of carbon film on the surface of macroscopic KCl monocrystal.

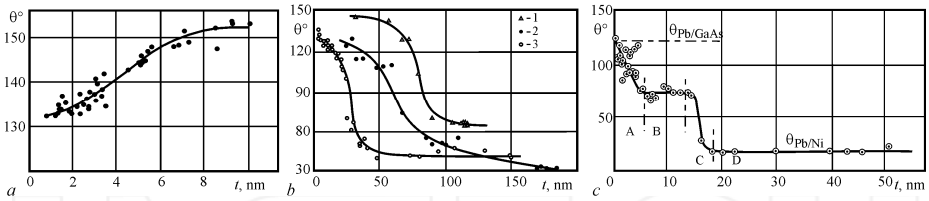

Figure 8. Wetting angle against thickness of intermediary film for systems Sn/C/KCl (a); Bi/Fe/KCl (1), Sn/Al/KCl (2), Pb/Ni/NaCl (3) (b); and Pb/Ni/GaAs (c) [9, 42–44, 63]

b. Systems with dissolution of film in liquid metal – Figure 7b. Dissolution of the material of intermediate film in liquid droplets causes considerable displacement of t_k toward the region of higher thickness values; examples of change of the wetting contact angle in such systems are given in Figure 8b. In this case the dependence features another typical thickness t_s, by which the intermediary film completely dissolves in the melt. The value t_s depends on the solubility of the film material in liquid metal at given temperature. A partial dissolution of film in liquid metal is observed within the interval of thickness $t_s < t < t_c$, which causes its discontinuity, that is, the substrate becomes heterogeneous. Since solubility of film material in the melt for the investigated systems is limited, the degree of substrate

heterogeneity is a function of film thickness, which fact accounts for the observed dependence $\theta(t)$. Dependencies of this type are observed in Pb/Ni/NaCl, Bi/Fe/KCl, Sn/Al/KCl systems (Figure 8b) and for a number of systems studied in [62]: [Cu, Ag, Pb, Sn]/[Mo, V, Fe]/[quartz, sapphire, graphite];

c. **Systems with chemical interaction of film with substrate**– Figure 7c (Pb/Ni/Si и Pb/Ni/GaAs [42, 63], Figure 8c). As could be seen from Figure 8c, in the Pb/Ni/GaAs system changes in wetting occur in two stages. First, the contact angle decreases to intermediary $\theta \approx 75°$, then over the range of thickness $6 < t < 14$ nm the plot $\theta(t)$ features a plateau, which has never been observed in similar systems investigated earlier, and further the contact angle changes again until it reaches a value corresponding to the Pb/Ni system. This variation of $\theta(t)$ directly suggests the presence of at least two mechanisms of wetting variation with film thickness, one of which occurs on the interval $0 < t < 14$ nm, and the other one at $t > 14$ nm. Hence, this type of system can be divided into two subsystems, and, accordingly, is specified by the two values of critical thickness. The second subsystem (regions B, C, D in Figure 8c) belongs to type (a) or (b). In the first subsystem substrate heterogeneity on the transition segment $0 < t < t_{c1}$ (region A in Figure 8c) is caused by the growth of new phase island – a chemical combination of film with substrate (results of phase analysis of double-layer Ni–GaAs films produced in different conditions are presented in works [64, 65]), and the value t_{c1}, which corresponds to the formation of continuous film of the compound, is defined by the mechanism of interaction of intermediate layer with substrate.

It should be noted that plots presented in Figure 7 are simplest and influence other factors, for example, interaction with the residual atmosphere (Sn/Al/KCl [42]) may cause a more complex variation of the contact angle with changing thickness of the intermediary film.

3.3. Wetting of thin free films

When interpreting results of wetting in three-component systems liquid–thin film–bulk substrate, it is difficult to separate effects due to film thickness itself and the influence of bulk substrate. Therefore, it was considered expedient to investigate wetting of thin free films depending on their thickness [42–44]. The obtained results did not make it possible to find size dependence of surface energies of thin carbon films. However, these results are of interest in themselves because it is possible for highly dispersed systems, when liquid particles wet not the surface of bulk solid bodies, but that of free thin films. In this case, specific effects connected to deformation of film under the liquid droplet are observed.

A theory of half-space wetting was constructed in [55]. It suggests that the droplet deforms the region near the line of contact of three phases to form a welt. In case of thin films deformation may be significant that makes it possible to find it by experiment. Therefore, in the following text we give an outline theoretical analysis of wetting of thin free films on assumption of constant surface energies σ_l, σ_u and σ_{ul}, made in work [54], and respective experimental results of the research [42–44].

http://dx.doi.org/10.5772/60900

3.3.1. Wetting of elastically deformed film with small droplets

According to [42–44, 54], the equilibrium characteristic of the system comprised of free elastically deformed film with the thickness t and the wetting droplet (Figure 9) is found in the same way as in the problem discussed earlier – from the minimum free energy condition, with introduction to the expression of which a summand corresponding to energy of the film:

$$F = 2\pi \int_0^L \left\{ \left[-p\left(z-\zeta\right) + \sigma_l \sqrt{1-z'^2} + \left(\sigma_{ul} - \sigma_u\right)\sqrt{1+\zeta'^2} \right] \rho\Theta\left(r-\rho\right) + \right.$$
$$\left. + 2\sigma_u \rho \sqrt{1+\zeta'^2} + \psi\left(\zeta', \zeta'', u, u', \rho\right) \right\} d\rho, \tag{19}$$

where L is the radius of the film fixation circle, functions $\zeta(\rho)$ and $z(\rho)$ define the radial profile of the surfaces of the film and the droplet, respectively; $\Theta(x)$ is the Heaviside step function.

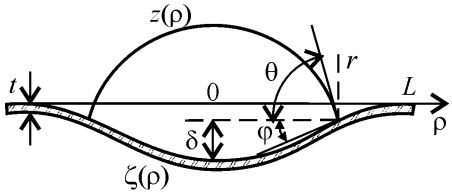

Figure 9. Schematic diagram of a liquid droplet on a thin elastic film

The function ψ is equal to the sum of contributions of elastic energies of pure bending ψ_1 and longitudinal extension of the film ψ_2, written, according to [66], with regard to axiality in the following form:

$$\psi_1 = \frac{1}{2} D\rho \left(\zeta'' + \frac{2\nu}{\rho}\zeta''\zeta' + \frac{1}{\rho^2}\zeta'^2 \right),$$
$$\psi_2 = \frac{6}{t^2} D\rho \left(u'^2 + \frac{2\nu}{\rho}u'u + \frac{u^2}{\rho^2} + \frac{1}{4}\zeta'^4 + u'\zeta'^2 + \frac{\nu}{\rho}u\zeta'^2 \right), \tag{20}$$

where ν is Poisson's ratio, u is the radial component of two-dimensional displacement vector, $D = Et^3/[12(1-\nu^2)]$ is the stiffness factor (E is Young's modulus).

The shape of the free surface of liquid is found by variation of the functional F in δz on $0 \le \rho \le r$. Upon double integration, the relevant Euler equation yields function $z(\rho)$ as a sphere (16) with the radius $R = 2\sigma_l/p$.

Variation of F in $\delta\xi$ and δu allows to obtain equations to define film deformation, which, after partial integration and substitution of the ψ_1 and ψ_2 from (20), assume the form

$$\zeta''' + \frac{1}{\rho}\zeta'' - \frac{1}{\rho^2}\zeta' - \frac{12}{t^2}\left(u' + \frac{\nu}{\rho}u + \frac{1}{2}\zeta'^2\right) - \\ -\frac{1}{D}\left[\left(\sigma_{ul} - \sigma_u\right)\Theta\left(r-\rho\right) + 2\sigma_u\right]\frac{\zeta'}{\sqrt{1+\zeta'^2}} = -\frac{pr}{2D}\Theta\left(r-\rho\right); \tag{21}$$

$$u'' + \frac{1}{\rho}u' - \frac{1}{\rho^2}u = -\zeta'\zeta'' - \frac{1-\nu}{2\rho}\zeta'^2. \tag{22}$$

The boundary conditions for equations (21) and (22) follow from non-integral summands of the variation δF going to zero. Two of them were used to draw equations (21), (22), and the rest may be written as follows: $u(0) = 0$; $\xi'(0) = 0$; $\xi(L) = 0$; $\xi'(L) = 0$; $u(L) = 0$; besides that, the point $\rho = r$ shall require continuity of the functions $\zeta(\rho)$, $\zeta'(\rho)$, $u(\rho)$, $\zeta''(\rho)$, and $u'(\rho)$.

The condition of equilibrium value of the contact angle θ may be determined by variation of functional (19) with δr. Here we obtain an expression, which is Young's equation written along the tangent line to the film surface at point $\rho = r$: $\sigma_l \cos(\theta - \phi) = \sigma_u - \sigma_{ul}$, where $\phi = \mathrm{arctg}\zeta'(r)$ – film inclination angle at the point $\rho = r$. The same Young's equation corrected for elastic surface inclination angle was obtained in [55].

Another relation connecting ϕ and θ follows from equation (21) and boundary conditions at the point $\rho = r$:

$$\sigma_l \cdot \sin\theta = \left(\sigma_{ul} - \sigma_u\right)\sin\phi + D\left[\zeta'''\left(r+0\right) - \zeta'''\left(r-0\right)\right]. \tag{23}$$

As it is seen from (21) and (23), the contact angle depends on film deformation and is determined by the jump of the third derivative $\zeta(\rho)$ on the line of three-phase contact.

Features of deformation for small and big film deflections, that is, with prevailing bending and tensile deformation, respectively, were evaluated in [54]. In the case when the maximum film deflection δ is less than its thickness, equations (21) and (22) become linear, and their solution yields the following expression

$$\frac{E}{1-\nu^2} = \frac{9\sigma_l \cdot \sin\theta_\infty}{8t^3}\left(\lim_{r\to 0}\frac{\delta}{r^3}\right)^{-1}, \qquad \phi \sim \frac{4}{3}\frac{\delta}{r}, \tag{24}$$

which relates Young's module to parameters measurable by experiment. At greater film bends ($\delta > t$), approximate solutions of equations (21) and (22) can be obtained resulting in the estimation

http://dx.doi.org/10.5772/60900

$$\frac{\delta}{r} \sim \left(2\sigma_l \cdot \sin\theta_\infty / Et\right)^{1/3}. \tag{25}$$

In the case of a very thin film $t \le 10\sigma/E$ (this can be the case for films with low elastic modulus) its shape under the droplet tends to sphere with the radius $R_{ul} = r\left(\sigma_u + \sigma_{ul}\right)/\sigma_l \sin\theta$ and remains flat outside the droplet. Smooth transition from one shape to another takes place in a narrow region with the width of the order of film thickness, and the value of the contact angle $\theta = \lim_{t\to 0}\theta(t)$ is defined only by surface phase energies in accordance with the equations

$$\begin{aligned} &\sigma_l \cos\theta_0 + \left(\sigma_u + \sigma_{ul}\right)\cos\phi = 2\sigma_u; \\ &\sigma_l \sin\theta_0 = \left(\sigma_u + \sigma_{ul}\right)\sin\phi. \end{aligned} \tag{26}$$

3.3.2. Wetting of free carbon films with metal droplets

As already noted, experimental research of wetting of free amorphous carbon films of different thickness with island vacuum condensates aimed at obtaining data on surface energy of films was made in [42–44]. The research used test metals (In, Sn, Pb), which are inert to carbon films and forming with carbon films contact angles of 140°–150°.

Test samples were prepared by evaporation and condensation of carbon and metal in a vacuum of 10^{-6} mm Hg on carbon films of different thickness located on copper grids with the mesh size of 60 μm. During the experiment the temperature was kept above the melting point for the relevant metal. Carbon film thickness varied on the range of 4–30 nm, and the size of liquid metal particles was 30–500 nm and was limited, on the one hand, by the need to exclude size effect due to dispersity of the liquid phase, and by strength of carbon films on the other.

Electron microscope examination of profiles of crystallized metal droplets (Figure 10) revealed substantial difference in the shape of the interphase boundary droplet–substrate for micro-particles condensed on free films and films on a solid surface. The difference is that when the film is thin enough it gets deformed by the droplet (Figure 10), while in particles condensed on a solid surface, liquid–substrate interface remained flat.

For the analyzed systems it was determined that at $t < 30$ nm the contact angle decreases with film thickness (Figure 11). At $t > 30$ nm the angle θ approaches the constant value θ_∞ that corresponds to wetting of bulk material. Analysis of profiles of droplets on free films showed that the film is deformed by the droplet, with the degree of deflection being a function of thickness and becoming a factor at $t < 10$ nm.

The obtained results were interpreted in [42–44] within the framework of wetting of elastically deformable carbon films [54], whose basic concepts were given earlier. As follows from relations (24) and (25), at t = const the relation of maximum film deflection δ to the droplet base radius r will be different for cases with prevailing deformation of bending ($\delta \sim r^3$ at $\delta < t$) and stretching ($\delta \sim r$ at $\delta > t$).

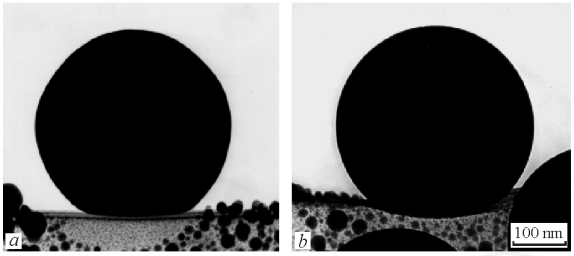

Figure 10. Micrographs of tin droplets on free carbon films with the thickness of 20 (a) и 10 (b) nm

Experimental relations δ(*r*) for the Sn/C system at *t* = 10 nm (Figure 12) corroborate this conclusion. It is apparent from the chart that the linear dependence δ(*r*) is observed at δ < *t* on the coordinates "r^3 — δ," and at δ > *t* – on the coordinates "*r* — δ."

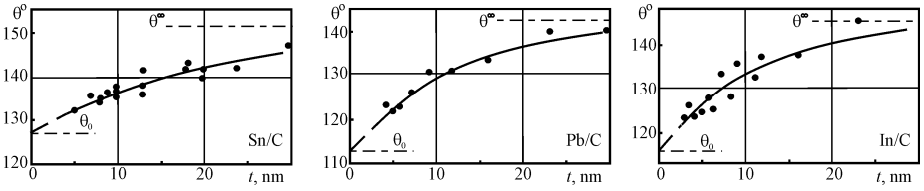

Figure 11. Dependence of the angle of wetting of free carbon films with tin (a), lead (b), and indium (c) on their thickness [42–44]

It follows from the same charts that $\lim_{r\to 0}(\delta / r^3) \mid_{\delta<t} = 7.5\cdot 10^{-6}$ nm^{-2} and $(\delta / r) \mid_{\delta>t} = 0.11$. Since Poisson's ratio is usually within the limits 1/4 < ν < 1/2, then from relation (24) one can estimate Young's modulus for carbon film, which turns out to be equal to $E \approx (3{,}4–4{,}2)\cdot 10^{10}$ N/m^2. With regard to this value from (25) one gets $(\delta / r) \mid_{\delta>t} \approx 0.10 \pm 0.01$, which agrees well with the experiment. Theoretical prediction of the contact angle at *t* = 10 nm, too, gives the value of θ = (140 ± 1)°, close to the experimental one of θ ≈ 138°.

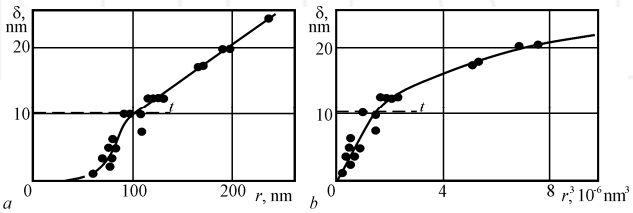

Figure 12. The relation δ(r) on the coordinates "r – δ" (a) and "r^3 – δ" (b) for tin droplets on a free carbon film with the thickness of 10 nm [42–44]

The results of theoretical consideration for very thin films were used to evaluate the surface energy of carbon films. As follows from (26) and (10), in the case when deformation energy in comparison with surface ones may be neglected, the quantity σ_u is defined by the expression

$$\sigma_u = \sigma_l \sin\theta_\infty \big/ 4\left(\cos\theta_0 - \cos\theta_\infty\right). \tag{27}$$

The range of free films thickness on which this relation is satisfied is not attainable experimentally (t < 1 nm); however, the angle θ_0 may be found by extrapolation of the relation $\theta(t)$. The values of carbon films surface energy estimated with the help of (27) from experimental data for the In/C, Sn/C, and Pb/C system make about 120 ± 30 mJ/m^2. Since data regarding surface energy of amorphous carbon films are unavailable, works [42–44] compare obtained values of σ_u with surface energy data for different modifications of carbon. Values of σ_u for carbon found by different authors quite well agree with the results [42–44], whereas large values of σ_u (500–2500 mJ/m^2) reported in literature, as a rule, refer to high temperature and crystalline modifications of carbon. It should be noted that great values of σ_u most likely cannot be taken as characteristics of amorphous carbon film because calculation of θ_0 even at σ_u = 350 mJ/m^2 gives values (130, 140 и 135° for In, Sn, and Pb, respectively) that exceed those measured experimentally.

Variation of θ with thickness of free films as a result of theoretically predicted size dependence of their surface energy is about an order of magnitude smaller than the change in the contact angle due to deformation. Hence, the studies did not allow to trace the dependence of $\sigma(t)$ for free carbon films, though they made it possible to determine the value of surface energy for them.

3.4. Wetting in supercooled island condensates

It is known that above the melting temperature the surface energy σ_l decreases linearly with increase of temperature. However, existing knowledge and experimental data on temperature dependence of surface energy of supercooled liquids are ambiguous [67]. According to [67] at significant supercooling values, one may expect inversion of the temperature dependence $\sigma_l(T)$.

The temperature dependence of the surface energy of metals (Ga, In, Sn, Bi, Pb) [68] has been studied only in the rage of small supercoolings down to $0.1T_s$. Using containerless electrostatic levitation techniques [69–71] for a number of refractory metals supercoolings $(0.12–0.18)T_s$ were reached and it was determined that the dependence $\sigma_l(T)$ is linear ($d\sigma_l/dT$<0) in the supercooled region.

Measurement of surface energy of supercooled melts is hard to make because considerable supercoolings are normally obtained in microvolumes, and traditional methods to determine σl require large amount of melt [1, 40]. However, temperature dependence of surface energy on at $T < T_s$ can be estimated by analyzing wetting of the solid substrate with supercooled droplets.

3.4.1. Inversion of wetting temperature dependence in island films

Contact pairs being island films of tin, indium, bismuth, and copper on amorphous carbon substrates and indium on aluminum substrate were investigated in [42, 43, 72]. The test samples were prepared by condensation in a vacuum of $5 \cdot 10^{-6}$–$2 \cdot 10^{-8}$ mm Hg on the circular substrate with temperature gradient (200–900 K) set along it. As a result, condensation to equilibrium or supercooled phase with the formation of microdroplets occurred according to the condensation diagram [73–76]. The obtained samples were cooled to room temperature and then wetting contact angles on crystallized droplets condensed at different substrate temperatures were measured. Due to wetting hysteresis, which occurs even on an absolutely smooth and uniform surface because of deformation of the substrate in the region of triple contact [60], the droplet base radius remains constant during cooling. The contract angles were measured on electron microscope pictures of droplet profiles (Figure 13) and averaged for 10–20 droplets. As long as condensation takes place on a substrate with temperature gradient, the relation $\theta(T)$ can be measured in single experiment on a wide range of temperatures with arbitrarily small temperature step.

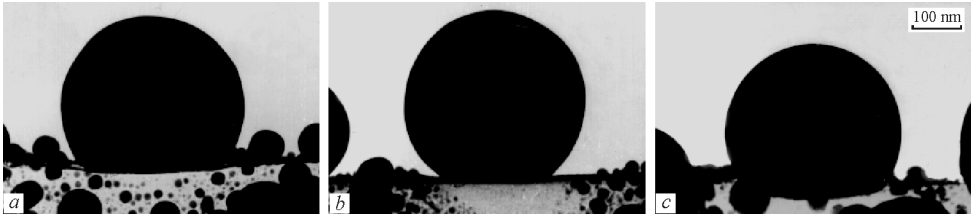

Figure 13. Micrographs of tin particles condensed in a vacuum of $5 \cdot 10^{-6}$ mm Hg at temperatures 400 K (a), 570 K (b), and 730 K (c) [72]

The results of measurement of wetting angles in the Sn/C and In/C systems [72] are presented in Figure 14a, b. The obtained dependencies are characterized by the maximum at temperatures 550 and 500 K for tin and indium, respectively. Below T_s the wetting angle gradually decreases with decrease of temperature. Decrease of θ for the investigated systems makes about 25° at maximum achieved supercoolings $\Delta T_{Sn} = 160$ K и $\Delta T_{In} = 100$ K. Better wetting is also observed above T_s at growing temperature, where for indium and tin θ decreases on the same temperature range: $550 < T < 650$ K. Over 700 K the contact angle in the Sn/C system shows behavior typical for noninteracting systems consisting in small decrease θ with the growth of temperature. Here the relation $\theta(T)$ is close to linear with the slope coefficient $d(\cos\theta)/dT \approx 0.0001$ K^{-1}.

In the Bi/C system temperature dependence of wetting, similarly to the In/C and Sn/C systems considered earlier, is nonmonotonic and is characterized by considerable decrease of the contact angle when approaching the temperature of maximum supercooling (Figure 14c). However, the maximum value of θ for bismuth is achieved at $T = 430$ K, that is, in supercooled state unlike tin and indium, for which the maximum $\theta(T)$ is above the melting temperature. The temperature range where the wetting angle decreases appears

http://dx.doi.org/10.5772/60900

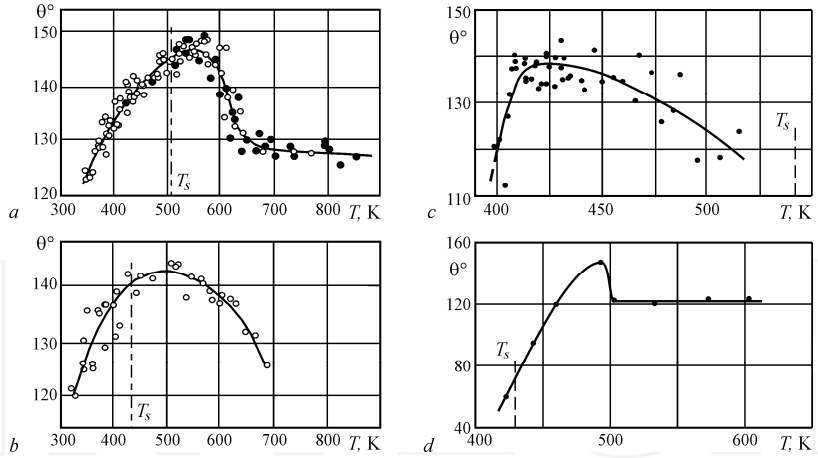

Figure 14. Temperature dependencies of wetting for island condensates of metals on different substrates. On the left – Sn/C (a) (base substrate: O – NaCl; ● – Al_2O_3; vacuum 5 10^{-6} mm Hg) and In/C (b), on the right – Bi/C (c), and In/Al (d) [42, 43, 72]

quite narrow: 400 < T < 420 K. On these interval θ decreases by 25°, this corresponds to reduction of adhesion tension by 50%.

Nonmonotonic dependence of the contact angle on temperature is also a feature of In/Al system (Figure 14d). This is similar to the relation θ(T) in the Sn/C system, but is almost completely above the melting temperature for indium. For In/Al relatively low supercoolings ($\Delta T/T_s \approx 0.05$) were received, which is generally typical for metal condensates on metal substrates [73, 74, 76]. Starting with the temperature T = 420 K (θ = 60°), the contact angle is growing with the growth of temperature, and at T = 490 K takes the maximum value of θ = 143°. It is followed by fast reduction of θ, and at T > 500 K the contact angle is constant with the value θ = 120°. Characteristically, at the melting temperature and below, in supercooled state, indium wets aluminum substrate. Transition from wetting to nonwetting, that is, the change of sign of adhesion tension, in the In/Al system is observed at T = 440 K.

For the Cu/C system wetting temperature dependence does not have any peculiarities: on the interval 1200 < T < 1300 K decrease of the contact angle is observed with growing temperature ($d(\cos\theta)/dT \approx 0.001$ K^{-1}). This, on the one hand, is similar to the behavior of θ(T) for the Bi/C system with the same values of relative supercoolings, and on the other the linear relation θ(T) is typical for contact systems with noninteracting components [1, 40].

Observed changes of the contact angle in the supercooled region, as noted in [42, 43, 72], is probably stipulated by abnormal behavior of either liquid metal surface energy or interface energy of the metal–carbon boundary. If σ_{ul} is assumed to be constant or growing with decrease of temperature, then according to Young's equation experimental data for θ(T) is an evidence of sharp increase in liquid metal surface energy. Thus, for tin at $T \leq 400$ K the variable σ_l, found

under assumption of constant adhesion tension, exceeds the relevant quantity for solid metal. Hence, crystallization of tin at $T < 400$ K will be accompanied by decreasing surface energy, which is not in agreement with existing theoretical models and experimental data. In this way, the assumption regarding constant let alone growing σ_{ul} with increasing supercooling leads to a contradiction. Therefore, the data for wetting in supercooled stated most likely suggest significant decrease of interfacial energy of the supercooled droplet–substrate boundary with decreasing temperature. The relations $\sigma_{ul}(T)$, calculated using linear extrapolation of the data for surface energy temperature dependence of liquid tin and indium [68] to the supercooling region, are presented in Figure 15.

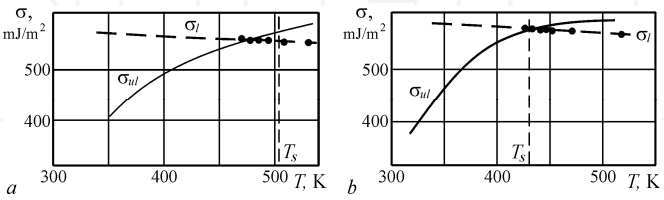

Figure 15. The plots of liquid phase surface energy [68] and interfacial energy of the droplet–substrate boundary against temperature for Sn/C (a) and In/C (b).

Among the reasons causing such a significant decrease in interfacial energy works [42, 43, 72] cite adsorption of gaseous impurities, which value increases with decrease of temperature or inversion of the surface energy of metal in supercooled state. However, considering the fact that for a number of analyzed metals (In, Sn, Bi) inversion of wetting temperature dependence occurs within approximately the same temperature range, while in the Cu/C system at high temperature it was not found at all, one should probably consider the adsorption of impurities from residual gases that grows at such temperatures crucial and causing decrease of interfacial energy on the carbon substrate boundary with increased supercooling, and hence, better wetting observed experimentally. The increase of temperature of the substrate above 500–600 K increases σ_u of carbon film due to sharp reduction of absorption of gases on its surface, which results in better wetting.

3.4.2. Influence of pressure of residual gases on wetting of carbon substrate with tin

The experimental relations $\theta(T)$ (Figure 14) may not be explained by linear change of surface energies of the contacting phases. In addition, one of the possible explanations of nonmonotonous behavior of $\theta(T)$ is the influence of adsorbed gaseous impurities. For this reason, the works [42, 43, 77] investigated temperature dependencies of contact angles for island films of tin on carbon substrates, condensed under the controlled composition of the residual atmosphere.

The samples were prepared using the technique described earlier [72] at the pressure of residual gases of 10^{-7}–10^{-9} mm Hg. A mass spectrometer was employed to control residual atmosphere, and its content was changed by leaking gas into the unit pumped to a pressure

http://dx.doi.org/10.5772/60900

of 10^{-9} mm Hg. The wetting contact angles were measured on micrographs of particle profiles on rolled-up (Figure 16) or inclined (Figure 17) spots of carbon film (convolution and angular observation methods [41, 42]); the quantity θ for a fixed temperature was found by averaging the contact angle values for 10–20 microparticles.

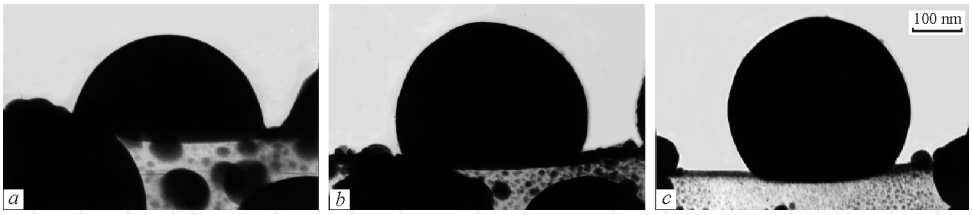

Figure 16. Micrographs of crystallized tin droplets condensed in a vacuum of $2 \cdot 10^{-8}$ mm Hg on carbon substrates at temperatures 350 K (a), 410 K (b), and 500 K (c) [42, 43, 77]

The results of measurement of $\theta(T)$ for tin droplets obtained under different vacuum are presented in Figure 18. Comparison of experimental data on wetting in tin films prepared in a vacuum of 10^{-6} и 10^{-8} mm Hg shows that they are different, firstly, by absence of a maximum in dependence $\theta(T)$ (pressure 10^{-8} mm Hg) and, secondly, by the fact that with better vacuum this dependence shifts to the region of smaller values of wetting angles (for pressure of 10^{-8} mm Hg this displacement makes 20–30°).

At substrate temperatures $T > 500$ K for films prepared in a vacuum of 10^{-8} mm Hg, relation $\theta(T)$ goes constant, and the contact angles become approximately equal to the angles θ for films produced at $p = 10^{-5}$ mm Hg, but at temperatures above 650 K. This suggests that the maximum on the wetting temperature dependence for island condensates of tin, indium, and bismuth obtained in a vacuum of 10^{-5}–10^{-6} mm Hg [72] is defined by the influence of gaseous impurities adsorbed from residual atmosphere, which respectively modify surface energies of the contacting phases. It is typical that the relation $\theta(T)$ for films condensed in a vacuum of 10^{-7} mm Hg assumes intermediate position between the values obtained for samples at $p = 10^{-6}$ and 10^{-8} mm Hg.

It is worth noting that for a supercooled state of tin decrease of temperature in all cases leads to a decrease of the contact angles. At the pressure of residual gases of 10^{-8} mm Hg improvement of wetting gets quite significant and makes $\Delta\theta \approx 50°$. Variation of wetting with temperature is well illustrated by micrographs of particle profiles (Figure 16) and inclined spots of film near the temperature of maximum supercooling (Figure 17). In this case, as could be seen from the chart (Figure 18, Curve 3) and micrographs (Figs. 16, 17), transition from nonwetting ($\theta > 90°$, i.e., $\sigma_{ul} > \sigma_u$) to wetting ($\theta < 90°$, $\sigma_{ul} < \sigma_u$) is observed in the region of deep supercoolings (at $T < 350$ K). Existence of such transition, which is essentially a change of sign of the adhesion tension σ_u–σ_{ul} directly corroborates the conclusion about significant decrease in interfacial energy of the droplet–substrate supercooling boundary with temperature, which is determined by adsorption of impurities from residual gases growing with decrease of temperature [42, 43, 72]. The results in work [77] give reason to assume that nonmonotonous wetting

dependence in the Sn/C system is due to the interaction of methane group gases produced in the process of operation of the hetero-ion pumping system.

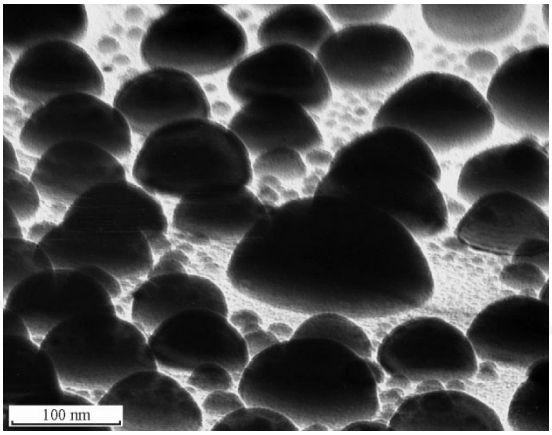

Figure 17. Micrographs of tin island film condensed in a vacuum of $2 \cdot 10^{-8}$ mm Hg on a carbon substrate at the temperature of 315 K ($\theta = 82°$)

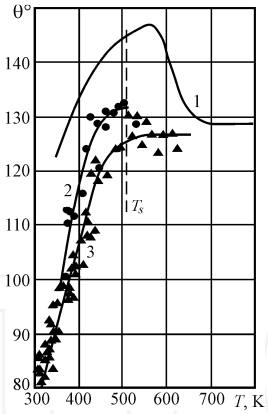

Figure 18. Temperature dependence of the contact angle of wetting of carbon substrates with tin islands prepared under different pressure of residual gases: 1 – $5 \cdot 10^{-6}$ mm Hg [72], 2 – $3 \cdot 10^{-7}$ mm Hg, and 3 – $2 \cdot 10^{-8}$ mm Hg. [42, 43, 77]

The analysis of the outlined results allows us to assume that the supercooled state of the metal itself is not the main cause of sharp improvement of wetting with decrease of temperature for fusible metals. This is also suggested by the fact that inversion of wetting temperature dependence is observed both above (Sn/C, In/C, In/Al) and below (Bi/C) of melting point, while for the Cu/C system there is no inversion at all. However, this conclusion may not be consid-

ered final since for the Cu/C system the relation $\theta(T)$ was studied at insignificant relative supercoolings ($\Delta T/T_s \approx 0.12$), and, probably, this is why wetting inversion was not detected. In this way, data available now suggest the generality of wetting inversion, though they are not sufficient to give a definite answer to the question regarding its mechanism.

3.4.3. Size effect in wetting in supercooled droplets

As it has been shown earlier using the contact systems (Sn/C, In/C, Bi/C, Pb/C, Au/C, Pb/Si) as a case study, wetting of amorphous neutral substrates with liquid metals is improving with decrease of the size of microdroplets [9, 42–44]. This effect is a result of decrease in surface energy of metal droplets σ_l themselves and droplet–substrate interfacial energy and has been only investigated for temperatures above the melting point of the metal. At the same time it is known that crystallization of small particles takes place at significant supercoolings [73–76], and for description of this process we must know both absolute values of the contact angles at relevant temperatures and their size dependence.

Such investigations for island tin films on amorphous carbon substrate were made in [72, 78]. The results of measurement of contact angles in the Sn/C system at temperatures 400 K and 315 K are presented in Figure 19, which shows that for supercooled droplets as well as for equilibrium ones (see Figure 6a) the contact angle decreases with decrease of droplets size. However, numerical values of the contact angles for droplets of equal size turn out to be different, and the relation $\theta(R)$ (R is the droplet radius) for supercooled droplets is displaced to the region of lower values of θ by quantity $\Delta\theta \approx 15°$ and 55° for 400 K and 315 K, respectively.

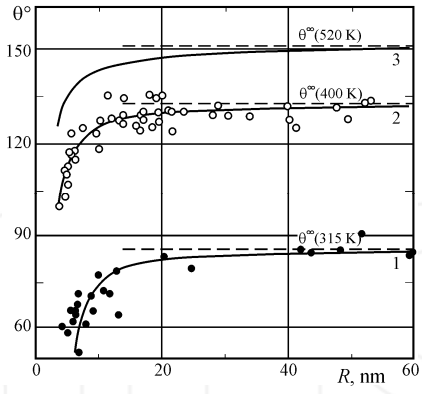

Figure 19. The plot of wetting angle against the radius of supercooled (1 – T = 315 K, 2 – T = 400 K [72, 78]) and equilibrium (3 – T = 520 K [9, 42–44]) tin microdroplets

Comparison with known results regarding the size effect of wetting at $T > T_s$ [9, 42–44] provides grounds to believe that the mechanism of the effect for metastable droplets (at $T < T_s$) is the same as for equilibrium ones, that is, it is defined by the dependence of the droplet–substrate interfacial energy on the size the droplet itself. This is also supported by the fact that obtained

dependencies $\theta(R)$ are linear in the coordinates "$\cos\theta - 1/R$," which is typical for the contact systems investigated earlier [9, 42–44]. Since extrapolation of surface energies to such significant supercoolings looks unjustified, it is not possible to numerically estimate size dependencies of surface and interface energies in the contact system. At the same time, the full similarity of relations $\theta(R)$ for equilibrium and supercooled particles offers grounds to argue that they are driven by the same laws.

4. Conclusions

The experimental data and their analysis outlined herein show that the application of island vacuum condensates to study surface energy and wetting allowed to obtain a number of general results of crucial importance for physics and chemistry of surface phenomena.

Quantitative data of surface energies of solid Au, Pb, and Bi nanoparticles and parameters that define size dependence of surface energy of small particles have been obtained from the investigations of evaporation processes in condensed films.

Options for measuring surface energy in the solid phase and its temperature dependence are discussed and are based on the data regarding the decrease of melting temperature of small metal particles. Temperature dependencies of surface energy for In, Sn, Bi, Pb, Al, Au, and Pt have been calculated on the basis of the preceding consideration. The significant reduction of surface energy for all metals studied when approaching melting temperature has been shown.

The detailed investigation and theoretical description of the size effect of wetting, which consists in the decrease of the wetting angle with the decrease of particles size, have been provided. Size dependencies of wetting angle in In/C, Sn/C, Bi/C, Pb/C, Pb/Si, and Au/C have been obtained for equilibrium and supercooled (Sn/C) liquid microdroplets. On the basis of these studies, size dependencies of interfacial energy of In/C, Sn/C, Bi/C, Pb/C, Au/C couples were obtained.

Experimental data and theoretical description of the effect of thickness of free carbon film on wetting angle have been obtained for In/C, Sn/C, and Pb/C couples. These studies enabled to determine the surface energy of thin carbon films, which makes $\sigma_u = 120 \pm 30$ mJ/m^2.

Temperature dependencies of contact angle in In/C, Sn/C, Bi/C, In/Al, and Cu/C couples have been obtained for equilibrium and supercooled liquid microdroplets.

Author details

Sergei Dukarov, Aleksandr Kryshtal* and Vladimir Sukhov

*Address all correspondence to: aleksandr.p.kryshtal@univer.kharkov.ua

V.N. Karazin Kharkiv National University, Kharkiv, Ukraine

References

[1] Adamson AW, Gast AP. Physical Chemistry of Surfaces. New Delhi: Wiley India; 2012.

[2] Bormashenko EYu. Wetting of Real Surfaces. Berlin: De Gruyter; 2013.

[3] Fisher IZ. Statistical Theory of Liquids. Chicago: University of Chicago Press; 1964.

[4] Geguzin YaE, Ovcharenko NN. Surface energy and surface processes in solids. Soviet Physics Uspekhi 1962; 5(1): 129–157. doi:10.1070/PU1962v005n01ABEH003403

[5] Kumikov VK, Khokonov KhB. On the measurement of surface free energy and surface tension of solid metals. J. Appl. Phys. 1983; 54: 1346–1350. doi:10.1063/1.332209.

[6] Sambles JR. An electron microscope study of evaporating gold particles: the Kelvin equation for liquid gold and the lovering of the melting point of solid gold particles. Proc. Roy. Soc. Lond. A 1971; 324: 339–350.

[7] Sambles JR, Skinner LM, Lisgarten ND. An electron microscope study of evaporation small particles. Proc. Roy. Soc. Lond. A 1970; 318(3): 507–522.

[8] Larin VI. Determination of surface energy of small particles from their evaporation. Funct. Mater. 1998; 5(1): 104–109.

[9] Larin VI. Capillary characteristics of thin films and small particles. Funct. Mater. 1998; 5(2): 145–164.

[10] De Gennes PG. Wetting: statics and dynamics. Rev. Mod. Phys. 1985; 57: 827–863.

[11] Tolman RC. The effect of droplet size in surface tension. J. Chem. Phys. 1949; 17: 333–337.

[12] Kirhwood JG, Buff FF. The statistical mecanical theory of surface tension. J. Chem. Phys. 1949; 17(2): 338–343.

[13] Magomedov MN. Dependence of the surface energy on the size and shape of a nanocrystal. Phys. Solid State 2004; 46(5): 954–968.

[14] Lu HM, Jiang Q. Size-dependent surface energies of nanocrystals. J. Phys. Chem. B 2004; 108(18): 5617–5619.

[15] Sdobnyakov NYu, Samsonov VM, Bazulev AN, Kuplin DA, Sokolov DN. The solubility region of Ga in PbTe films prepared on Si-substrates by modified "hot wall" technique. Funct. Mater. 2011; 18(2): 181–188.

[16] Xiong S, Qi W, Cheng Y, Huang B, Wang M, Li Yejun B. Modeling size effects on the surface free energy of metallic nanoparticles and nanocavities. Phys. Chem. Chem. Phys. 2011; 13(22): 10648–10651.

[17] Chamaani A, Marzbanrad E, Rahimipour MR, Yaghmaee MS, Aghaei A, Kamachali RD, Behnamian Y. Thermodynamics and molecular dynamics investigation of a pos-

sible new critical size for surface and inner cohesive energy of Al nanoparticles. J. Nanopart. Res. 2011; 13: 6059–6067.

[18] Zadumkin SN, Khokonov KhB. Surface energy of thin metal films. Fiz. Met. Metalloved. 1962; 13: 658–663.

[19] Shebzukhova G, Arefieva LP, Khokonov KhB. Dimensional dependence of the surface energy of thin cadmium films. Bull. Russ. Acad. Sci. Phys. 2012; 76(10): 1133–1135.

[20] Shcherbakov LM, Samsonov VM, Bazulev AN. The application of thermodynamic perturbation theory to the calculation of excess free energy of small systems: 1. The study of the dimensional dependence of specific free energy of small droplets. Colloid J. 2004; 66(6): 760–765.

[21] Samsonov VM, Sdobnyakov NY, Bazulev AN. Size dependence of the surface tension and the problem of Gibbs thermodynamics extension to nanosystems. Colloids Surf. A: Physicochem. Eng. Aspects 2004; 239: 113–117.

[22] Buffat Ph, Borel JP. Size effect on the melting temperature of gold particles. Phys. Rev. A 1976; 13(6): 2287–2298.

[23] Asoro MA, Kovar D, Ferreira PJ. In-situ transmission electron microscopy observations of sublimation in silver nanoparticles. ACS Nano 2013; 7(9): 7844–7852.

[24] Nanda KK, Kruis FE, Fissan H. Evaporation of free PbS nanoparticles: evidence of the Kelvin effect. Phys. Rev. Lett. 2002; 89: 256103-1-4.

[25] Nanda KK, Maisels A, Kruis FE et al. Higher surface energy of free nanoparticles. Phys. Rev. Lett. 2003; 91: 106102.

[26] Vogelsberger W, Marx G. Zur Krummung sabhangigkeit der Oberflach enspanung kleiner Tropfchen. Z. Phys. Chem. Leipzig 1976; 257(3): 580–586.

[27] Mei QS, Lu K. Melting and superheating of crystalline solids: from bulk to nanocrystals. Progress Mater. Sci. 2007; 52(8): 1175–1262. doi:10.1016/j.pmatsci.2007.01.001

[28] Kryshtal AP, Sukhov RV, Minenkov AA. Critical thickness of contact melting in the Au/Ge layered film system. J. Alloys Compounds 2012; 512: 311– 315.

[29] Gladkikh NT, Kryshtal'AP, Sukhov RV. Contact melting in layered film systems of the eutectic type. Phys. Solid State 2010; 52(3): 633–640.

[30] Gladkikh NT, Bogatyrenko SI, Kryshtal AP, Anton R. Melting point lowering of thin metal films (Me = In, Sn, Bi, Pb) in Al/Me/Al film system. Appl. Surf. Sci. 2003; 219: 338–346.

[31] Wronski CRM. The size dependence of the melting point of small particles of tin. Brit. J. Appl. Phys. 1967; 18: 1731–1737.

[32] Berman RP, Curzon AE. the size dependence of the melting point of small particles of indium. Canad. J. Appl. Phys. 1974; 52: 923–929.

[33] Peppiat SJ. The melting of small particles. I. Lead. Proc. Roy. Soc. Lond. A 1975; 345: 387–399.

[34] Peppiat SJ. The melting of small particles. II. Bismush. Proc. Roy. Soc. Lond. A 1975; 345: 401–412.

[35] Allen GL, Bayles RA, Gile WW, Jesser WA. Small particle melting of pure metals. Thin Solid Films 1986; 144(2): 297–308.

[36] Skripov VP, Koverda VP, Skokov VN. Size effect on melting of small particles. Phys. Status solidy (a) 1981; 66: 109–118.

[37] Pawlow PJ. Uher die Ahhangigkeit des Schmeltzpunktes von der Oberflachenenergie eines festen Korpers. Z. Phys. Chem. 1909; 65: 1–35, 545–548.

[38] Lu HM, Jiang Q. Surface tension and its temperature coefficient for liquid metals. J. Phys. Chem. B 2005; 109: 15463–15468.

[39] Morokhin VA, Pastukhov BA, Khlynov BB, Furman EL. Temperature dependence of the surface energy of iron. Poverkhnost. Fizika, Khimia, Mekhanika (Surface. Physics, Chemistry, Mechanics). 1987; 9: 121–125.

[40] Jaycock MJ, Parfitt GD. Chemistry of Interfaces. New York: Halsted Press; 1986.

[41] Gladkikh NT, Chizhik SP, Larin VI, Grigoryeva LK, Dukarov SV. Methods of determination of wetting in highly dispersed systems. Phys. Chem. Mech. Surfaces 1987; 4(11): 3465–3482.

[42] Gladkikh NT, Dukarov SV, Kryshal OP, Larin VI, Sukhov VN. Kapillyarnye svojstva ostrovkovykh plenok i malykh chastits (Capillary Properties of Island Films and Small Particles). Kharkiv: V. N. Karazin Kharkiv National University; 2015.

[43] Gladkikh NT, Dukarov SV, Kryshal OP, Larin VI, Sukhov VN, Bogatyrenko SI. Poverkhnostnye yavleniya i fazovye prevrashcheniya v kondensirovannykh plenkakh (Surface Phenomena and Phase Transformations in Condensed Films). Kharkiv: V. N. Karazin Kharkiv National University; 2004.

[44] Chizhik SP, Gladkikh NT, Larin VI, Grigorieva LK, Dukarov SV. Size effects in wetting for highly dispersed systems. Phys. Chem. Mech. Surf. 1987; 4(12): 3707–3724.

[45] Gladkikh NT, Grigor'eva LK, Dukarov SV et al. Size and temperature dependences of the surface tension of ultradisperse metallic particles. Sov. Phys. Solid State 1989; 31(5): 728–733.

[46] Yuan Y, Lee TR.contact angle and wetting properties. Surf. Sci. Tech. 2013; 5: 13–34.

[47] Amirfazli A, Chatain D, Neumann AW. Drop size dependence of contact angles for liquid tin on silica surface: line tension and its correlation with solid–liquid interfacial tension. Colloids Surf. A: Physicochem. Eng. Aspects 1998; 142: 183–188.

[48] Heine DR, Grest GS, Webb EB. Surface wetting of liquid nanodroplets: droplet-size effects. Phys. Review Lett. 2005; 95(10): 107801. doi:10.1103/PhysRevLett.95.107801

[49] Eustathopoulos N, Jound J. Interfacial tension and adsorption of metallic systems. Curr. Topics Mater. Sci. 1980; 4: 281–360.

[50] Larin V, Borodin A. Dimentional effect at wetting in Au–C system. Funct. Mater. 2001; 8(2): 309–313.

[51] Kryshtal AP. Formation of island arrays by melting of Bi, Pb and Sn continuous films on Si substrate. Applied Surf. Sci. 2014; 321: 548–553.

[52] Kryshtal AP, Gladkikh NT, Sukhov RV. Features of island nanostructures formed by melting Sn, Bi and Sn–Bi thin films on C substrates. Appl. Surf. Sci. 2011; 257: 7649–7652.

[53] Dukarov SV, Petrushenko SI, Sukhov VN, Churilov IG. Effect of temperature on the pores growth in the polycrystalline films of fusible metals. Prob. Atomic Sci. Technol. 2014; 1(89): 110–114.

[54] Rozenbaum VM, Dukarov SV, Gladkikh NT. Wetting by small droplets of free elastically deformable film. Poverkhnost. Fizika, Khimia, Mekhanika (Surface, Physics, Chemistry, Mechanics). 1989; 1: 104–112.

[55] Rusanov AI. On the theory of wetting of elastically deformable solids. Kolloidnyj zhurnal (Colloid Journal) 1977; 39(4): 704–710.

[56] Borodin AA, Gladkikh NT, Dukarov SV. Size effect on wetting of elastically deformable substrate. Vestnik KhGU, Fizika (V. N. Karazin Kharkiv State University Bulletin. Series of Physics). 1998; 417(1): 110–113.

[57] Kryshtal AP, Bogatyrenko SI, Sukhov RV, Minenkov AA. The kinetics of the formation of a solid solution in an Ag-Pd polycrystalline film system. Appl. Phys. A 2014; 116(4): 1891–1896.

[58] Minenkov AA, Bogatyrenko SI, Sukhov RV, Kryshtal AP. Size dependence of the activation energy of diffusion in multilayer Cu-Ni films. Phys. Solid State 2014; 56(4): 823–826.

[59] Bogatyrenko SI, Gladkikh NT, Kryshtal'AP, Samsonik AL, Sukhov VN. Diffusion in nanodisperse layered film systems. Phys. Metals Metall. 2010; 109(3): 255–260.

[60] Borodin AA, Dukarov SV. Wetting angle hysteresis in condensed microdrops. Funct. Mater. 2002; 9(3): 498–501.

[61] Eral HB, Mannetje DJCM't, Oh JM. Contact angle hysteresis: a review of fundamentals and applications. Colloid Polym. Sci. 2013; 291(2): 247–260.

[62] Naidich YuV, Kostyuk BD, Kolesnichenko GA, Shaikevich SS. Adhesion properties and wetting by molten metal of thin metallic films applied to nonmetallic materials. Sov. Powder Metall. Met. Ceram. 1973; 12(12): 988–993.

[63] Gladkikh NT, Dukarov SV. Lead wetting of thin nickel films deposited onto GaAs. Funct. Mater. 1996; 3(1): 97–99.

[64] Dukarov SV. γ-Phase structure in Ni-Ga-As thin film system. Funct. Mater. 1997; 4(3): 355–358.

[65] Gladkikh NT, Grebennik IP, Dukarov SV. Effect of condensation conditions on phase formation in thin two-layer Ni/GaAs films. Funct. Mater. 1998; 5(1): 44–47.

[66] Landau LD, Lifshitz EM. Theory of Elasticity. Oxford/Boston: Butterworth-Heinemann; 1995.

[67] Croxton CA. Liquid State Physics – A Statistical Mechanical Introduction. New York: Cambridge University Press; 2009.

[68] Zadumkin SN, Ibragimov KhI, Ozniev DT. Study of the surface tension and density of supercooled tin, indium, bismuth, lead and gallium. Izvestiya Vysshikh Uchebnykh Zavedenij. Tsvetnaya Metallurgiya 1979; (1): 82–85.

[69] Ishikawa T, Okada JT, Paradis P-F, Watanabe Y. Thermophysical property measurements of high temperature melts using an electrostatic levitation method. Jpn. J. Appl. Phys. 2011; 50(11S): 11RD03 doi:10.1143/JJAP.50.11RD03.

[70] Okada JT, Ishikawa T, Watanabe Y, Paradis P-F. Surface tension and viscosity of molten vanadium measured with an electrostatic levitation furnace. J. Chem. Thermodynam. 2010; 42(7): 856–859. doi:10.1016/j.jct.2010.02.008.

[71] Paradis P-F, Ishikawa T, Koike N. Thermophysical properties of molten yttrium measured by non-contact techniques. Microgravity Sci. Technol. 2009; 21(1–2): 113–118. doi: 10.1007/s12217-008-9074-8.

[72] Dukarov SV. Size and temperature effects on wetting in supercooled vacuum condensates. Thin Solid Films 1998; 323(1–2): 136–140.

[73] Gladkikh NT, Dukarov SV, Sukhov VN. Investigation of supercooling during metal crystallization under conditions close to weightlessness using island vacuum condensates. Z. fur Metallkunde 1996; 87(3): 233–239.

[74] Gladkikh NT, Dukarov SV, Sukhov VN. Overcooling on metal crystallization in island-like vacuum deposited films. Fizika Metallov i Metallovedenie 1994; 78(3): 87–93.

[75] Gladkikh NT, Dukarov SV, Sukhov VN, Churilov IG. Condensation mechanism of AgCl and NaCl island films on a nickel substrate. Funct. Mater. 2011; 18(4): 529–533.

[76] Gladkikh NT, Dukarov SV, Kryshal OP, Larin VI. Size effect upon solidification of small bismuth particles. Phys. Metals Metallurg. 1998; 85(5): 536–541.

[77] Dukarov SV, Gladkikh NT, Borodin SA. Temperature dependence of wetting in supercooled tin condensates at a carbon substrate. Fizicheskaya inzheneriya poverkhnosti (Physical Surface Engineering) 2003; 1(1): 89–93.

[78] Dukarov SV. Size effect on wetting in a supercooled island films of Sn. Adgeziya rasplavov i payka materialov (Adhesion of Melts and Brazing of Materials) 2010; 43: 3–11.